

Supplementary figure 1

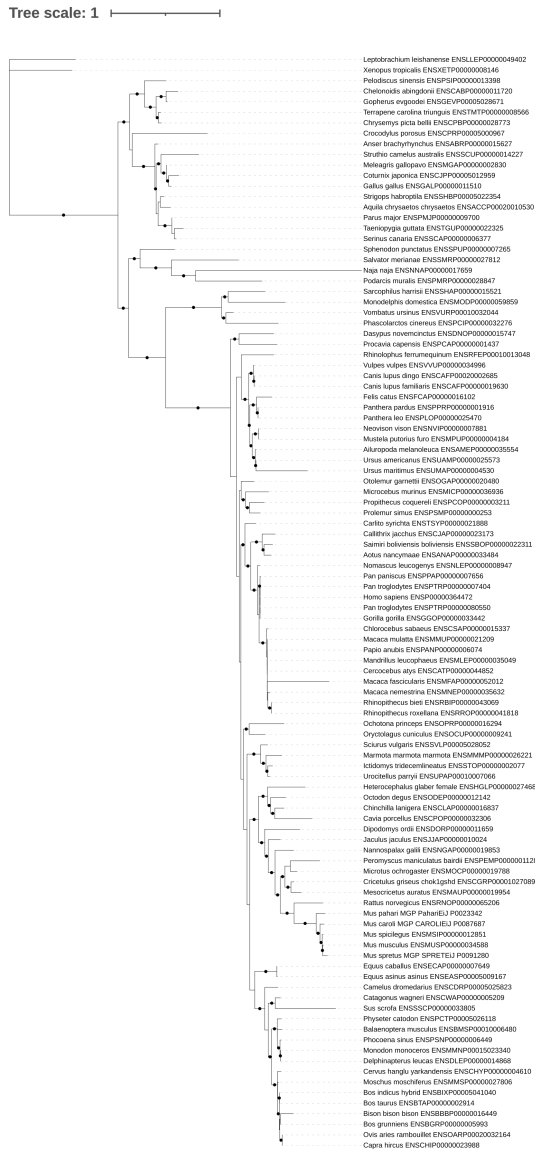
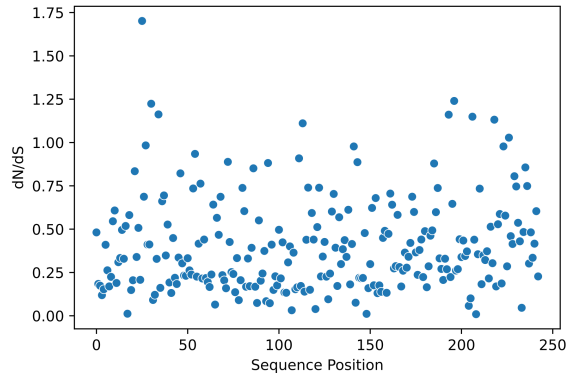


Figure 1: Maximum likelihood phylogeny inferred from a multiple sequence alignment of sarcopterygian apoA-I sequences. Black dots indicate node support values greater than 90% (calculated using 1000 replicates of UltraFast Bootstrap).

Supplementary figure 2

A



B

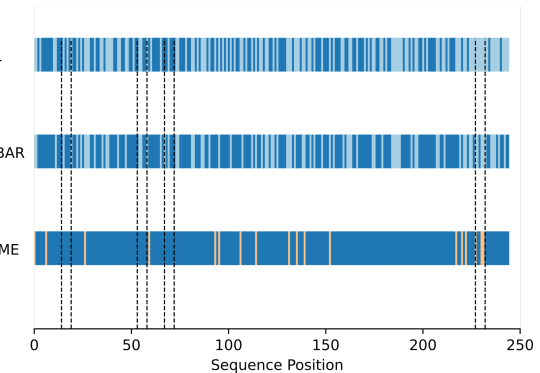
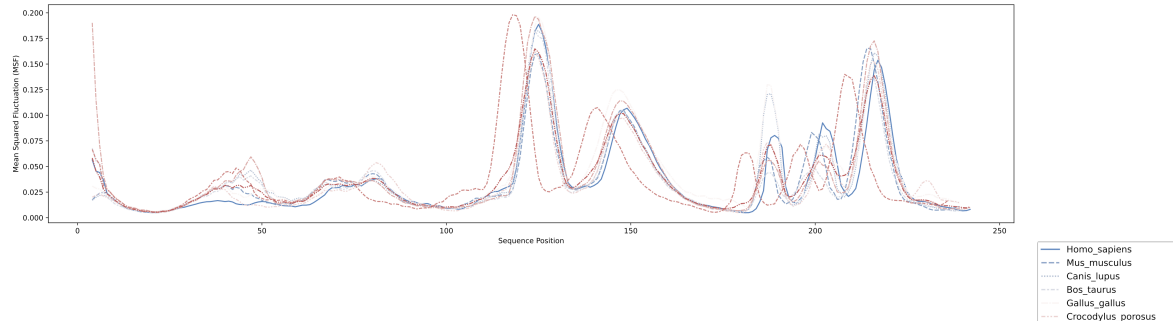


Figure 2: **A** Evolutionary rate (dN/dS) for each residue in the apoA-I codon alignment. **B** Cartoon depicting the evidence of adaptive evolution for each site of apoA-I sequence; residues under purifying, neutral and diversifying selection are colored in blue, paleblue and orange, respectively.

Supplementary figure 3

A



B

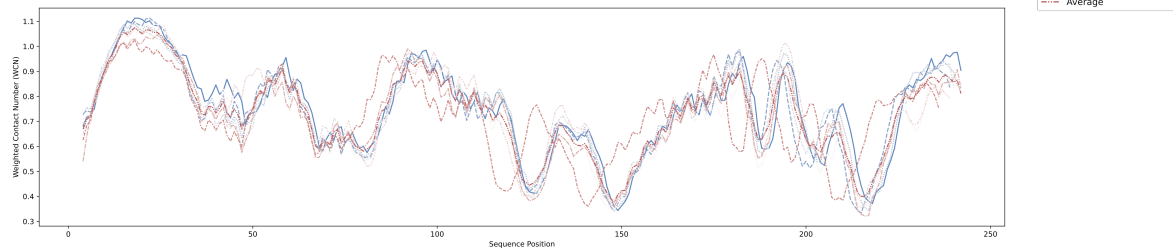


Figure 3: **A** Mean squared fluctuation (MSF) and **B** weighted contact number (WCN) profiles computed for each modelled structure

Supplementary figure 4

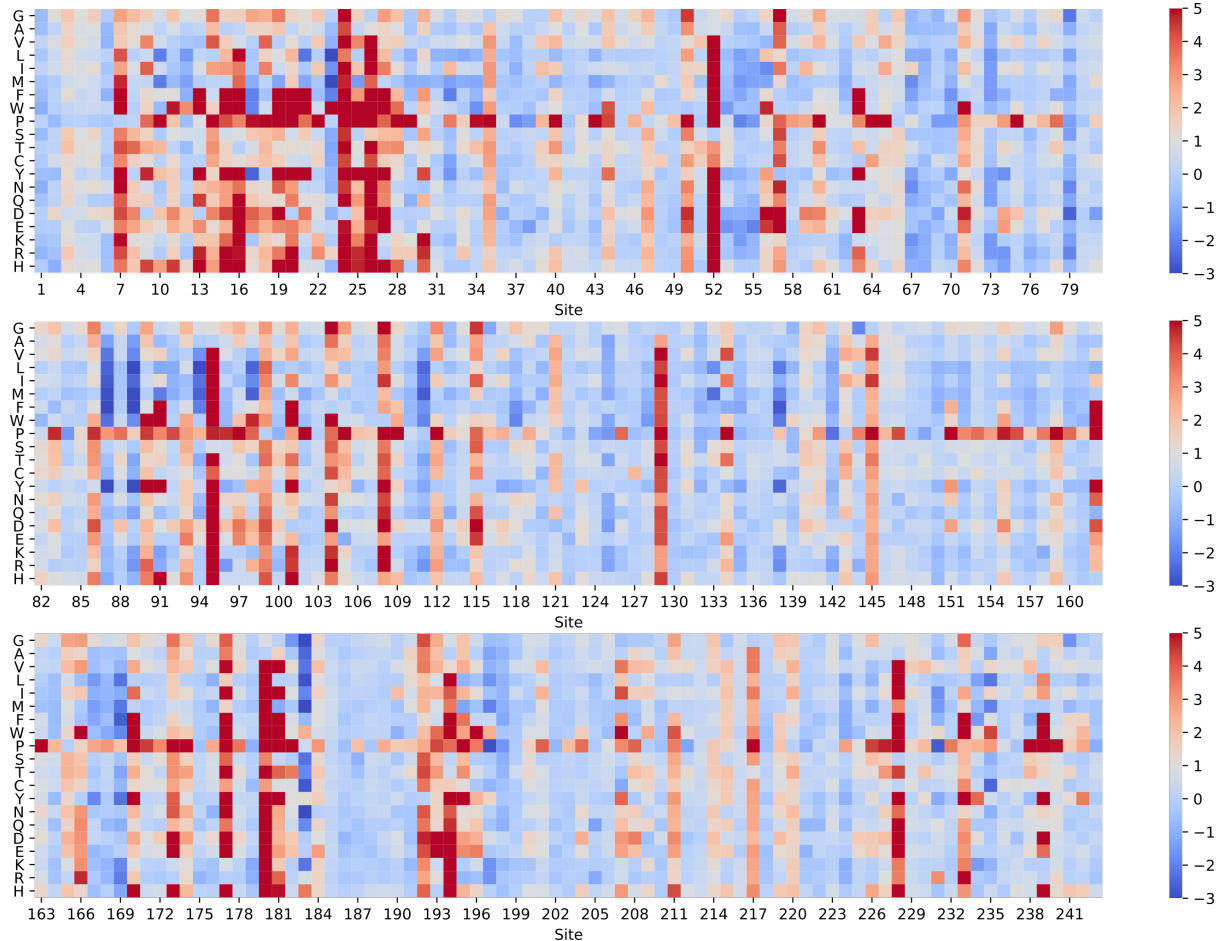


Figure 4: FoldX thermodynamic destabilization landscape. $\Delta\Delta G$ values obtained by *in silico* saturation mutagenesis of apoA-I structure using the FoldX engine. Mutation introduced is depicted in the Y axis. Scales at the right indicate $\Delta\Delta G$ values expressed in kcal/mol.

Supplementary figure 5

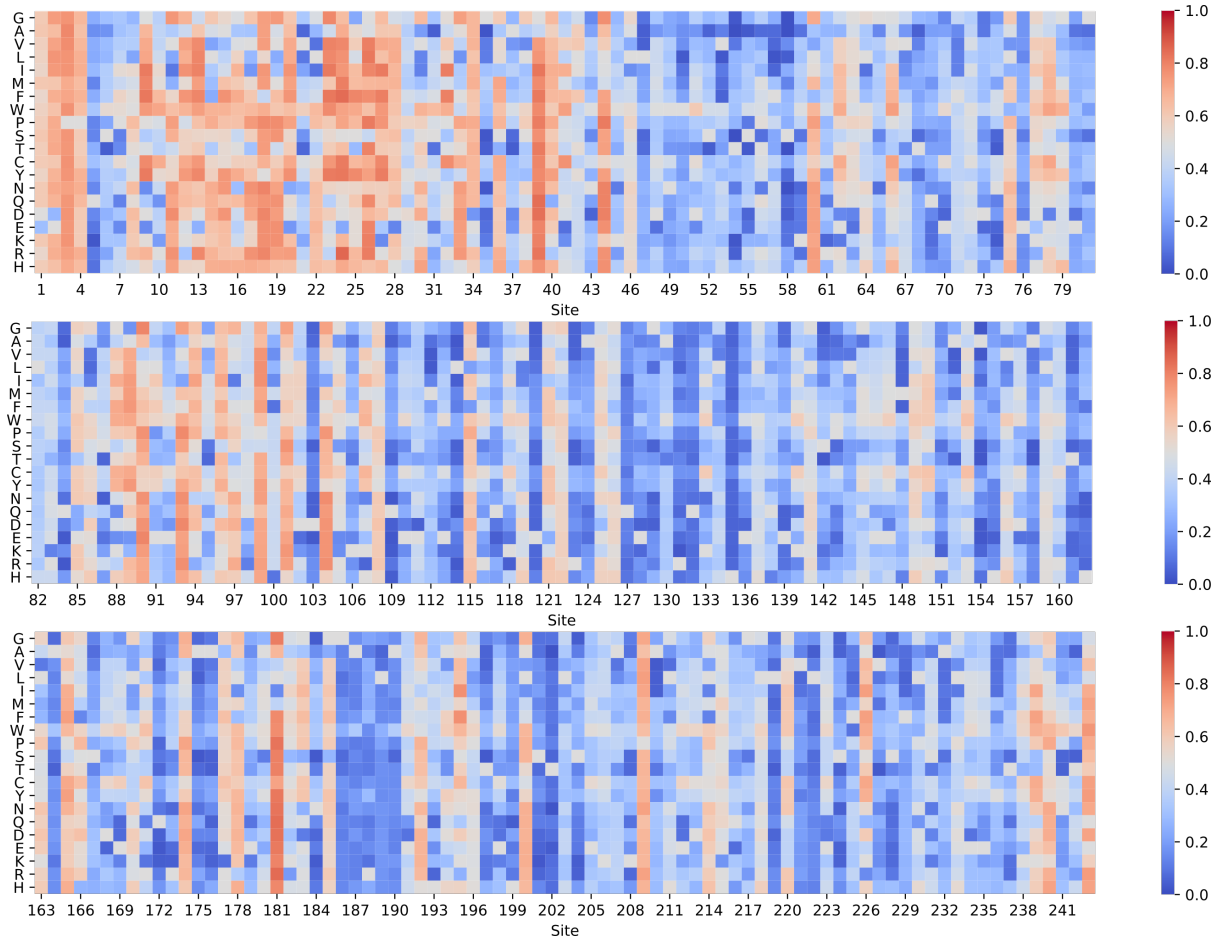


Figure 5: Rhapsody pathogenicity landscape. Pathogenicity values obtained by *in silico* saturation mutagenesis of apoA-I structure using the Rhapsody package. Mutation introduced is depicted in the Y axis. Scales at the right indicate pathogenicity score (1 more pathogenic, 0 less pathogenic)

Supplementary figure 6

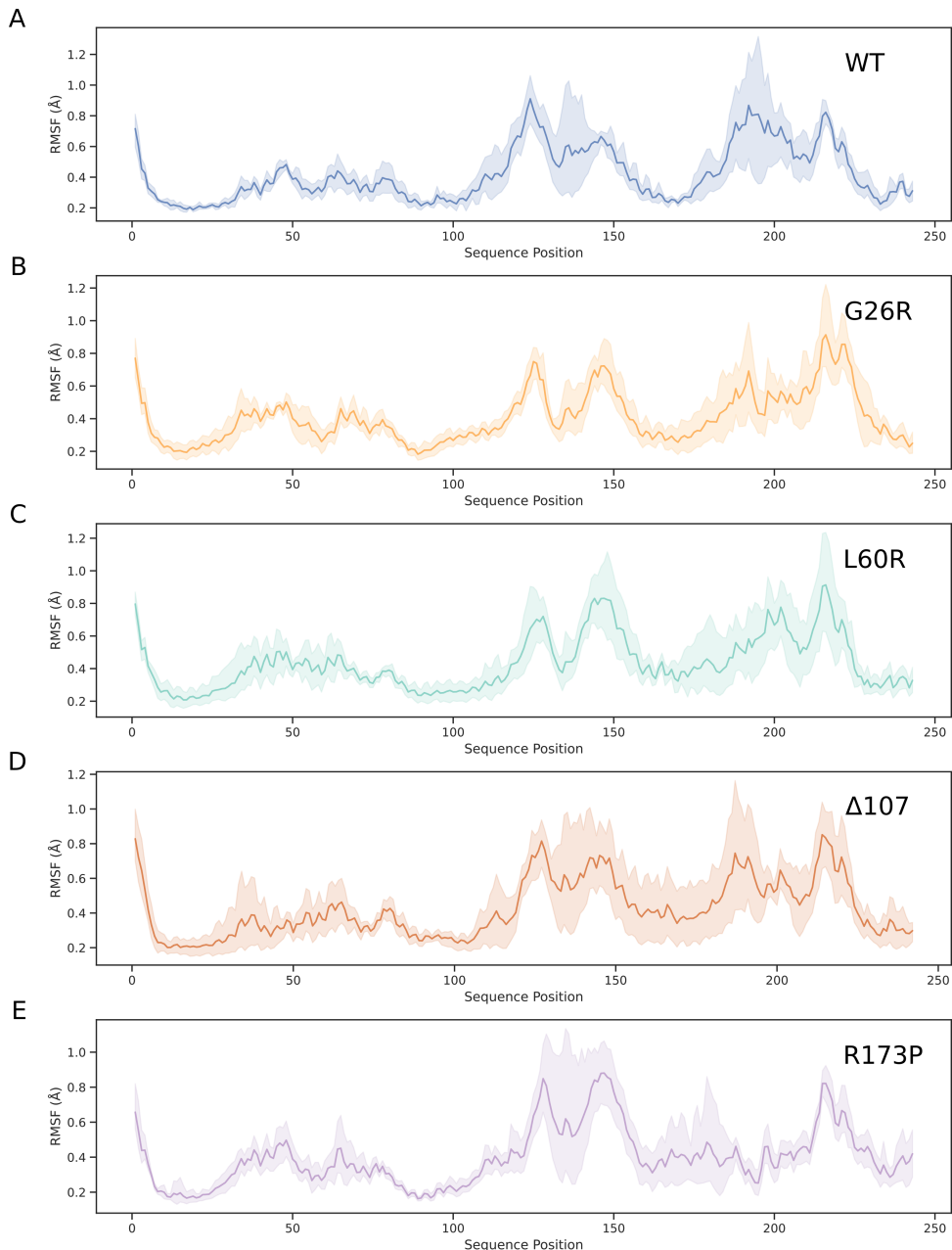


Figure 6: **A-E** Root mean square fluctuation (RMSF) profiles for apoA-I mutants. RMSF values were computed for each protein position over the last 100 ns of the simulation. Mean values are depicted together with its standard deviation.

Supplementary figure 7

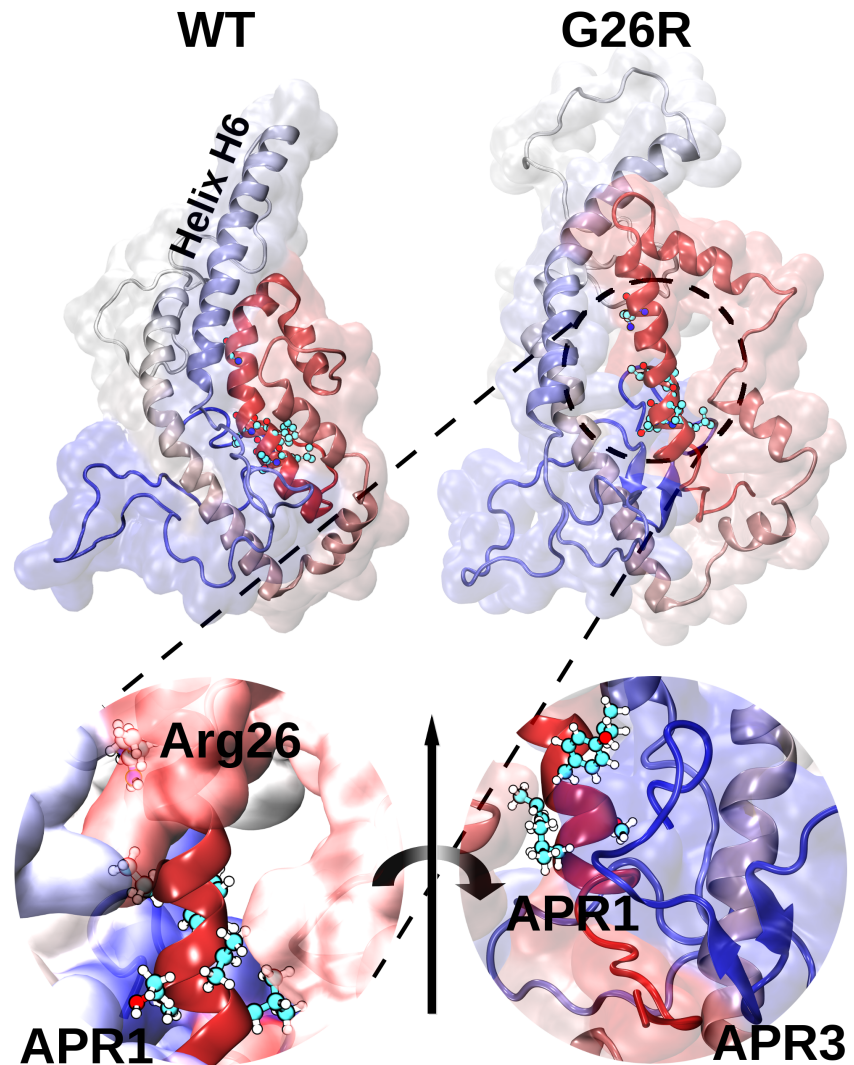


Figure 7: Graphical representation of the consensus model (WT) and the final snapshot of one of the replicas simulated for the G26R mutant. The substitution of glycine by arginine in position 26 destabilizes the helix bundle, expelling helix H6 with the concomitant solvent exposure of APR1 (left inset). A 180° view rotation shows the beta-sheet hairpin formed between residues S224 and A232, corresponding to the APR4 (right inset).

Supplementary table 1

Table 1: Aggregation score for each aggregation-prone region within apoA-I amyloidosis-associated mutants.

Variant	Aggregation_score	APR
wt	352.767	APR1
G26R	352.767	APR1
E34K	352.767	APR1
W50R	352.767	APR1
L60R	352.767	APR1
L64P	352.767	APR1
F71Y	352.767	APR1
L75P	352.767	APR1
L90P	352.767	APR1
L170P	352.767	APR1
R173P	352.767	APR1
L174S	352.767	APR1
A175P	352.767	APR1
L178H	352.767	APR1
L178P	352.767	APR1
L178R	352.767	APR1
K238N	352.767	APR1
wt	6.44347	APR2
G26R	6.44347	APR2
E34K	6.44347	APR2
W50R	6.44347	APR2
L60R	6.44347	APR2
L64P	6.44347	APR2
F71Y	6.44347	APR2
L75P	6.44347	APR2
L90P	6.44347	APR2

Variant	Aggregation_score	APR
L170P	6.44347	APR2
R173P	6.44347	APR2
L174S	6.44347	APR2
A175P	6.44347	APR2
L178H	6.44347	APR2
L178P	6.44347	APR2
L178R	6.44347	APR2
K238N	6.44347	APR2
wt	0	APR3
G26R	0	APR3
E34K	0	APR3
W50R	0	APR3
L60R	0	APR3
L64P	0	APR3
F71Y	0	APR3
L75P	0	APR3
L90P	0	APR3
L170P	0	APR3
R173P	0	APR3
L174S	0	APR3
A175P	0	APR3
L178H	0	APR3
L178P	0	APR3
L178R	0	APR3
K238N	0	APR3
wt	32.6745	APR3
G26R	32.6745	APR3
E34K	32.6745	APR3
W50R	32.6745	APR3
L60R	32.6745	APR3
L64P	32.6745	APR3

Variant	Aggregation_score	APR
F71Y	32.6745	APR3
L75P	32.6745	APR3
L90P	32.6745	APR3
L170P	32.6745	APR3
R173P	32.6745	APR3
L174S	32.6745	APR3
A175P	32.6745	APR3
L178H	32.6745	APR3
L178P	32.6745	APR3
L178R	32.6745	APR3
K238N	32.6745	APR3

Supplementary table 2

Table 2: Root mean square deviation (angstroms) computed for each apoA-I system.

System	Replicate_1	Replicate_2	Replicate_3	Replicate_4	Replicate_5	Mean	SD
wt	7.91	7.24	8.04	5.39	7.92	7.3	1.11
G26R	6.75	10.33	7.54	7.65	6.1	7.67	1.61
L60R	6.61	6.11	10.28	8.3	7.87	7.83	1.63
Δ 107	7.28	6.84	7.77	6.03	8.79	7.34	1.03
R173P	8.97	8.24	7.14	6.91	8.16	7.88	0.85